Sensors and Actuators A xxx (2013) xxx–xxx

Contents lists available at SciVerse ScienceDirect

Sensors and Actuators A: Physical

journal homepage: www.elsevier.com/locate/sna

High temperature micro-glassblowing process demonstrated on fused quartz and ULE TSG

D. Senkal, M.J. Ahamed, A.A. Trusov*, A.M. Shkel

MicroSystems Laboratory, 4200 Engineering Gateway Building, Department of Mechanical and Aerospace Engineering, University of California, Irvine, CA 92697, United States

ARTICLE INFO

Article history:
Received 17 August 2012
Received in revised form
27 November 2012
Accepted 28 November 2012
Available online xxx

Keywords:
Micro-glassblowing
3-D MEMS
Fused quartz
Ultra low expansion titania silicate glass

ABSTRACT

We report, for the first time, a MEMS fabrication process for building atomically smooth, symmetric 3-D wineglass and spherical shell structures, using low internal loss materials, namely fused quartz and ultra low expansion titania silicate glass (ULE TSG). The approach consists of three major steps: (1) a deep fused quartz cavity etch, (2) plasma activated bonding of fused quartz to fused quartz or TSG and (3) a high temperature (up to 1700 °C) micro-glassblowing process. An in-house process capability of 1800 °C glassblowing with a rapid cooling rate of 500 °C/min was developed. Feasibility of the process has been demonstrated by fabrication of fused quartz and TSG micro-glassblown structures. Spherical and inverted-wineglass shells with self-aligned stem structures were fabricated using this process. The approach may enable new classes of TSG and fused quartz MEMS devices with extremely low surface roughness (0.23 nm surface average), intrinsically low thermoelastic dissipation (Q_{TED} > 5E+10), and highly symmetric structures (radial error < 500 ppm).

1. Introduction

Maximization of the *Q*-factor is key to enhancing performance of vibratory MEMS devices in demanding signal processing, timing and inertial applications [1]. Current MEMS fabrication techniques limit the maximum achievable *Q*-factor by restricting the material choice to few materials and device geometry to 2-D planar structures. Available materials such as single-crystal silicon have relatively high thermoelastic dissipation and 2-D planar devices are mostly limited by anchor losses. The macro-scale Hemispherical Resonator Gyroscope (HRG) with *Q*-factors over 25E+6 [2] motivates the investigation of 3-D fused quartz micro-wineglass structures for use as vibratory elements in MEMS applications. This paper investigates the intriguing possibility of fused quartz micro-glassblowing as a means to fabricate 3-D shell micro-devices, Fig. 1.

With the emergence of novel fabrication techniques batch fabrication of 3-D wineglass structures are becoming possible. For instance, hemispherical shells fabricated by deposition of polysilicon [3] or silicon nitride [4] thin films into isotropically etched cavities have recently been demonstrated. Alternative fabrication techniques include "3-D SOULE" process for fabrication of mushroom and concave shaped spherical structures [5], as well as blow molding of bulk metallic glasses into pre-etched cavities [6]. MEMS wineglass resonators with atomic smoothness and low thermoelastic dissipation (TED) have not yet been demonstrated in the literature. To take full advantage of the 3-D wineglass architecture, fabrication techniques with low surface roughness as well as materials with high isotropy and low TED are desired.

It has been demonstrated that single-crystal silicon MEMS devices can reach the fundamental Q_{TED} limit by using a combination of balanced mechanical design and vacuum packaging with getters [7]. TED is caused by local temperature fluctuations due to vibration and the associated irreversible heat flow, which results in entropic dissipation. TED can be reduced either by decoupling the frequencies of mechanical vibrations from the thermal fluctuations or by using materials with low coefficient of thermal expansion (CTE). This paper focuses on materials with low CTE, such as fused quartz (0.5 ppm/°C) and ultra low expansion titania silicate glass (0.03 ppm/°C), which can provide a dramatic increase in fundamental Q_{TED} limit (Q_{TED} > 7E+10 for a TSG wineglass structure). When compared to silicon, titania silicate glass and fused quartz dry etching suffers from an order of magnitude higher surface roughness, lower mask selectivity, ~1 :1 for KMPR® photoresist and lower aspect ratio, <5:1 [8,9].

Pyrex glassblowing at 850 °C on a silicon substrate was previously demonstrated for fabrication of smooth, symmetric 3-D structures [10–13]. However, fused quartz/TSG glassblowing requires temperatures upwards of 1600 °C due to its higher softening point, which prevents the use of fabrication processes that rely on a silicon substrate. This paper explores the hypothesis that high temperature glassblowing (up to 1700 °C), may serve as an enabling mechanism for wafer-scale fabrication of TSG and

* Corresponding author. Tel.: +1 949 824 6314.
E-mail address: atrusov@uci.edu (A.A. Trusov).

0924-4247/$ – see front matter © 2013 Elsevier B.V. All rights reserved.
http://dx.doi.org/10.1016/j.sna.2012.11.040

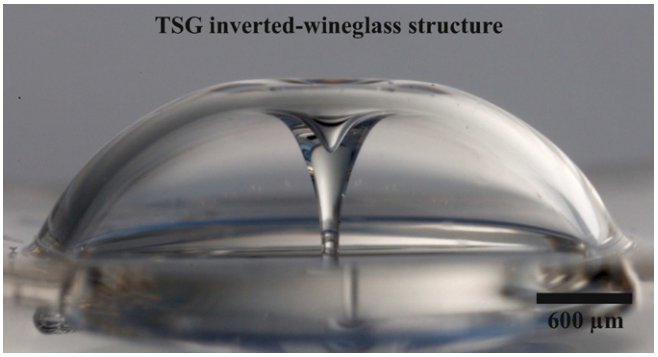

Fig. 1. Optical photograph of glassblown TSG inverted-wineglass structure. Outer diameter is 4200 µm. Glassblown at 1650 °C.

fused quartz 3-D wineglass structures. The approach consists of a high temperature micro-glassblowing process and an inverted-wineglass architecture that provides self-aligned stem structures. An in-house process capability of 1800 °C glassblowing with a rapid cooling rate of 500 °C/min was developed. Feasibility of the process has been demonstrated by fabrication of TSG and fused quartz micro-wineglass structures and spherical shells [14].

In the following sections, firstly the design parameters for micro-glassblowing is presented. This is followed by details of the fabrication process and the custom-designed fabrication equipment. The paper concludes with analysis of the glassblown structures and discussion of the results.

2. Design parameters

This section focuses on analysis of geometric design parameters and the effect of material choice on fundamental *Q*-factor limits. In order to establish the relationships between material choice, device dimensions and *Q*-factor, parametric Finite Element Analysis (FEA) was conducted using Comsol® Multiphysics Package [15].

2.1. Geometric design

Micro-glassblowing process utilizes an etched cavity on a substrate wafer and a glass layer that is bonded on top of this cavity, creating a volume of trapped gas for subsequent glassblowing of self-inflating spherical shells. When the bonded wafer stack is heated above the softening point of the structural glass layer, two effects are activated at the same time: (1) the glass layer becomes viscous, and (2) the air pressure inside the pre-etched cavity increases above the atmospheric level. This results in plastic deformation of the glass layer, driven by gas pressure and surface tension forces (glassblowing). The expansion of air (and hence the formation of the shell) stops when the pressure inside and outside of the glass shell reaches an equilibrium, creating a self-limiting process. During this deformation, the surface tension acting on the now viscous glass layer works towards minimizing the surface area of the structure as a result a highly symmetric spherical shell with low surface roughness forms. The process allows simultaneous fabrication of an array of identical (or different if desired) shell structures on the same substrate.

Shape and size of the final glassblown structure can be designed by changing starting conditions such as thickness of the device layer, cavity shape and dimensions as well as environment temperature and pressure during glassblowing [10]. For example, changing the cavity diameter directly affects the diameter of the final glassblown shell, whereas changing the cavity depth (or volume) affects the height of the glassblown structure. It is also possible to fabricate entirely different geometries by changing the initial conditions, for example a circular cavity creates a spherical shell when glassblown, Fig. 2 (right). Inverted-wineglass structures can also be fabricated by defining a central post inside the etched cavity, Fig. 2 (left). When the device layer is bonded to this central post, it acts as an anchor point, which allows the glassblown shell to fold around it, creating a self-aligned stem structure as in Fig. 2(e).

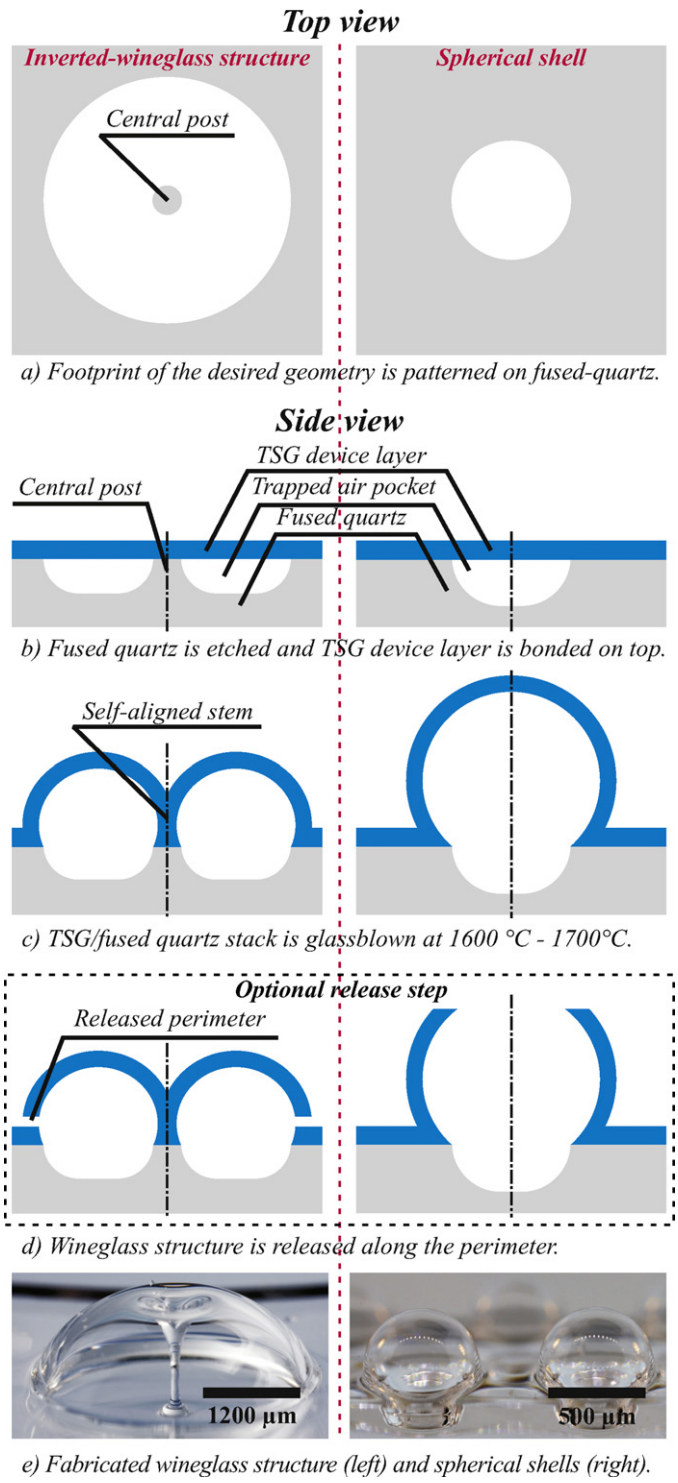

Fig. 2. ULE TSG/fused quartz micro-glassblowing process, consists of: (a) footprint of the desired geometry is patterned on fused-quartz, (b) fused quartz is etched and TSG device layer is bonded on top, (c) TSG/fused quartz stack is glassblown at 1600–1700 °C, (d) wineglass structure is released along the perimeter, and (e) fabricated wineglass structure (left) and spherical shells (right).

Please cite this article in press as: D. Senkal, et al., High temperature micro-glassblowing process demonstrated on fused quartz and ULE TSG, Sens. Actuators A: Phys. (2013), http://dx.doi.org/10.1016/j.sna.2012.11.040

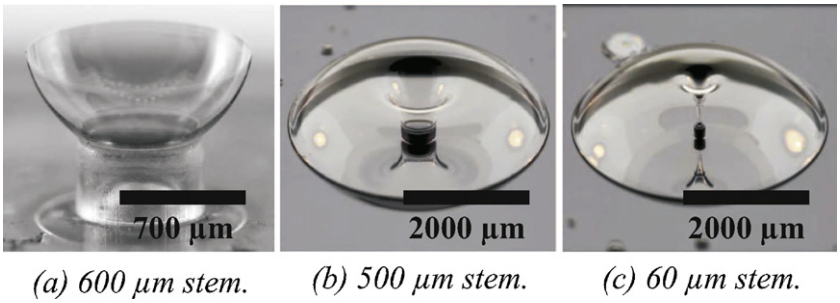

Fig. 3. Wineglass structures with (a) 1.2 mm outer diameter and 600 μm stem diameter (hollow), (b) 4200 μm outer diameter and 500 μm stem diameter (solid) and (c) 4200 μm outer diameter and 150 μm stem diameter (solid).

2.2. Stem design

Anchor loss is the dissipation of kinetic energy within the vibrating structure into the substrate and the environment by means of acoustic waves, which ultimately limits the overall *Q*-factor of the resonator. The focus of the analysis was to investigate the impact of stem diameter on Q_{anchor} and use the results of the FEA as design guidelines. Two types of geometries were analyzed: (1) Wineglass structures with hollow stem [13] shown in Fig. 3(a), and (2) inverted wineglass structures as in Fig. 3(b) and (c). The structure in Fig. 3(a) was fabricated by first glassblowing a spherical structure through a stencil layer and then cutting the top half of the spherical shell using laser ablation to create a wineglass structure. Whereas the structures in Fig. 3(b) and (c) were fabricated by etching a toroidal cavity as described in Fig. 2.

The structure in Fig. 3(a) had a shell diameter of 1142 μm, anchor diameter of 600 μm and average thickness of 4 μm, which gives roughly 1:2 attachment to shell diameter ratio. In contrast, the inverted-wineglass structures with the integrated stem, Fig. 3(b) and (c), had a shell diameter of 4200 μm, an average thickness of 80 μm with 500 μm and 150 μm stem diameters respectively, giving a 1:8 and 1:28 stem to shell diameter ratios.

To simulate the acoustic loss in an infinite medium, a perfectly matched layer (PML) within Comsol® Multiphysics Package [15] was used for modeling the substrate domain. PML works by absorbing acoustic waves over a large frequency range at any non-zero angle of incidence. The simulation was run for perfectly symmetric structures, neglecting the contribution of mass imbalance to the anchor loss. For this reason, the values obtained from FEA represent the fundamental anchor loss limit (theoretical maximum) of the structures (Table 1).

The wineglass structure with 1:2 anchor to shell diameter ratio, Fig. 3(a), had a fundamental Q_{anchor} limit of 3000, which is in close agreement with the experimentally obtained quality factor of 1256 [13]. Analysis of the wineglass structure with outer diameter ratio of 1:8 in Fig. 3(b) showed moderate anchor loss (fundamental Q_{anchor}> 2E+06). In contrast, the analysis of the wineglass structure with the integrated stem (1:14 ratio), Fig. 3(b), showed potential for significantly lower anchor loss (fundamental Q_{anchor}> 5E+10).

2.3. Thermoelastic dissipation

The goal of the analysis was to understand the effect of CTE on Q_{TED}. Four different materials: Silicon, pyrex, fused quartz and TSG were investigated using Comsol® Multiphysics Package [15]. Energy loss caused by TED was analyzed using a coupled thermo-mechanical model, where compressive and tensile stresses within the vibrating structure affected the temperature distribution and vice versa. Damping term was calculated as the total irreversible heat flow due to the change in the temperature distribution. The model was solved for the $n = 2$ wineglass modes, and Q_{TED} values were extracted from the ratio of the real and imaginary parts of the eigenfrequencies. It was found that the material choice has a significant impact on the Q_{TED} for the analyzed geometry (Table 2).

TSG, with the lowest CTE among the materials investigated, had the highest fundamental Q_{TED} value at 7E+10, which was followed by fused quartz at Q_{TED} > 2E+7.

3. Fabrication process and custom-designed fabrication equipment

3.1. Fabrication process

Fabrication process for TSG wineglass structures consists of four main steps, namely: (1) etching of the fused quartz (or fused silica) substrate, (2) bonding of fused quartz or TSG device layer to fused quartz, (3) glassblowing, and subsequently (4) releasing the wineglass structure by etching around the perimeter, Fig. 2. The process starts by LPCVD deposition of a 2 μm poly-silicon hard mask onto the fused quartz substrate. The cavity openings are defined on the PolySi hard-mask using RIE, followed by wet etching of ~150 μm deep toroidal cavities or ~300 μm deep cylindrical cavities into the substrate wafer using concentrated HF (49%). In order to establish the etch rate of HF on fused quartz and TSG, 75 min test runs were performed at room temperature. Etch depth was measured every 15 min by stopping the etch and measuring with a DEKTAK 3 profilometer. Linear regression fits showed an etch rate of 1.07 μm/min for fused quartz and 2.86 μm/min for TSG, with a linearity of $R^2 = 0.996$ and $R^2 = 0.997$, respectively. Once the etch was complete, PolySi layer was stripped and the wafers were thoroughly cleaned using RCA clean.

The next step of the fabrication process is bonding of the TSG device layer onto the etched fused quartz wafer. Due to the subsequent high temperature glassblowing process the bond needs to survive up to 1700 °C, which prevents the use of intermediate materials. For this reason, a plasma activated fusion bonding process was developed, Fig. 2(b). The bond is performed by plasma activating the TSG and fused quartz wafers and then bringing them into optical contact [16].

Table 1
Anchor loss analysis show a large change in Q_{anchor} for different stem diameters.

Stem diameter (μm)	600	500	60
Wineglass diameter (μm)	1200	4200	4200
Q_{anchor}	3E+03	2E+06	5E+10

Table 2
Thermoelastic dissipation analysis of micro-wineglass structures show that 3–6 orders of magnitude increase in Q_{TED} is achievable by using low expansion materials.

Material	Silicon	Pyrex	FQ	TSG
Q_{TED}	6E+04	7E+06	2E+07	7E+10

Please cite this article in press as: D. Senkal, et al., High temperature micro-glassblowing process demonstrated on fused quartz and ULE TSG, Sens. Actuators A: Phys. (2013), http://dx.doi.org/10.1016/j.sna.2012.11.040

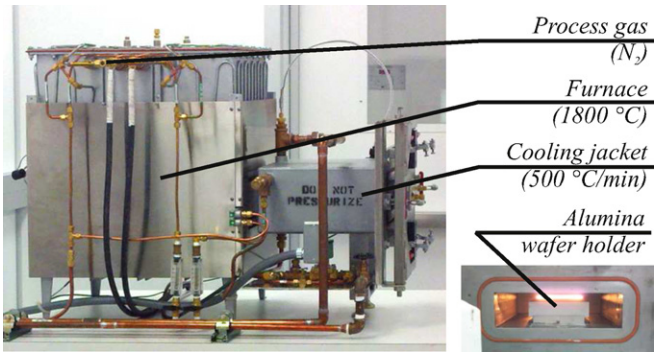

Fig. 4. Custom-designed furnace with process capability of 1800 °C glassblowing with a rapid cooling rate of 500 °C/min was developed.

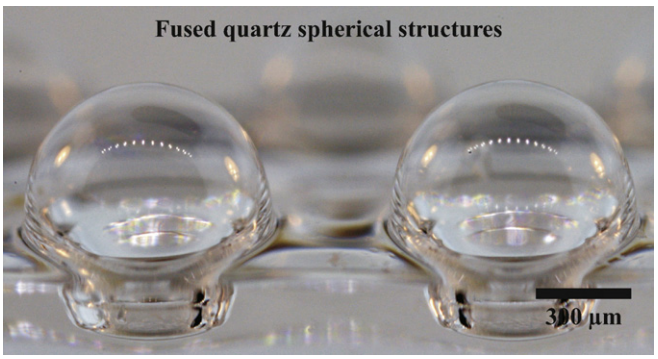

Fig. 5. Optical photograph of fused quartz spherical shell structures, glassblown at 1700 °C. Outer diameter of shells is 800 µm.

Plasma activated fusion bonding works by creating hydrogen bonds between the device and the substrate wafers, it requires highly polished, flat, clean surfaces (<1 nm roughness average). The process for bonding fused quartz or TSG wafer pairs can be divided into four main steps:

1. Cleaning of the wafer pair using solvent and RCA clean,
2. Plasma activation using oxygen plasma (50 W power for ~2 min, 24 sccm O_2 flow),
3. DI water rinse followed by N_2 dry and optical contacting of the activated surfaces,
4. Curing the wafer stack at 400 °C for 6 h.

Once cured, the bond creates a seamless hermetic seal around the etched cavities without using any intermediate material.

3.2. Custom-designed furnace

The TSG/fused quartz wafer stack is then glassblown at 1600–1700 °C in a custom-designed high temperature furnace with a rapid cooling rate of 500 °C/min, Fig. 4. The furnace consists of two main chambers that are connected to each other through a third vestibule chamber. The first chamber is used for heating and can go up to 1800 °C, the second chamber is enveloped by a water cooled jacket, that maintains < 200 °C temperature. The samples are transferred between the heating and cooling chambers by using a sliding alumina wafer holder. A typical glassblowing run involves keeping the wafer stack at glassblowing temperature for one minute and then extracting the wafer stack into the water cooled jacket for solidification.

During glassblowing, as previously described two phenomena occur simultaneously: device layer becomes viscous due to the elevated temperature and the air inside the etched cavity expands, creating the 3-D glassblown structure. Because the device layer is bonded both around the circular cavity and the cylindrical post in the middle, the glassblown structure creates a self-aligned stem, Fig. 1. Whereas if no central post is defined, the glassblown structure forms a spherical shell as in Fig. 5.

3.3. Laser ablation setup

The final step of the fabrication process is to release the wineglass around its perimeter, which can be accomplished by laser ablation or dry etching of the device layer. The wineglass structure in Fig. 6 was released with laser ablation, using a 2-axis laser micromachining system, Resonetics RapidX 250. 3-axis laser ablation capability was added by implementing a custom built rotary stage assembly from National Aperture, Inc. The wineglass structure was mounted onto the rotary stage and its axis of symmetry was aligned with the rotation axis using an x–y stage. Laser ablation was performed by focusing the laser beam onto the perimeter of the wineglass at a perpendicular angle and rotating the wineglass structure at constant angular velocity. For the laser source, an ArF excimer laser (193 nm wavelength, Coherent COMPexPRO 110) was used with 20 ns pulse duration, 50 Hz repetition rate and a laser spot size of 40 µm.

4. Analysis of structures

In this section the surface roughness and the material composition of TSG device layer before and after glassblowing and the symmetry of the fabricated glassblown structure is analyzed.

4.1. Surface roughness

In order to minimize the surface losses in resonant and optical applications highly smooth surfaces are required. Surface roughness measurements of TSG glassblown samples were performed using an atomic force microscope (AFM) from Pacific Nanotechnology (Nano-R). With a sensor noise level of <0.13 nm in the z-direction, Nano-R can resolve sub-nanometer features. Samples were cleaned using standard solvent clean (acetone, IPA, methanol) before each scan. No additional treatment was performed on the samples. The AFM was run in tapping mode, using a 10 nm radius probe tip (Agilent U3120A).

Surface roughness of the samples before and after glassblowing were analyzed, with the hypothesis that glassblowing can improve the surface roughness. Highly polished TSG wafers were used for the device layer, which was verified by AFM scans, showing a surface roughness of 0.40 nm Sa, Fig. 7(b). Characterization of the

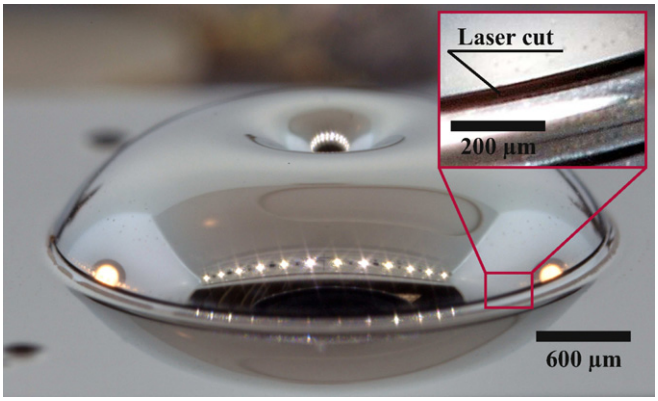

Fig. 6. Optical photograph of inverted-wineglass, released along the perimeter using laser ablation and coated with iridium.

Please cite this article in press as: D. Senkal, et al., High temperature micro-glassblowing process demonstrated on fused quartz and ULE TSG, Sens. Actuators A: Phys. (2013), http://dx.doi.org/10.1016/j.sna.2012.11.040

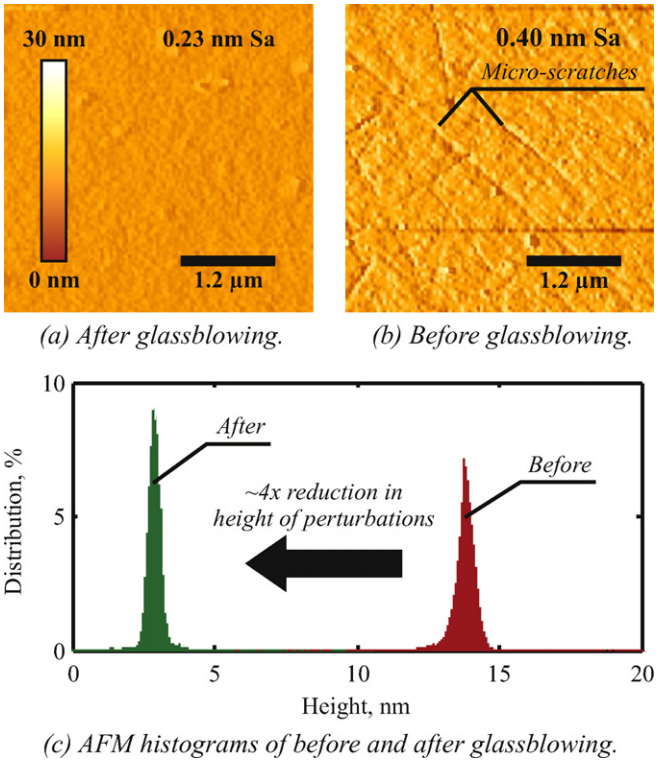

Fig. 7. AFM surface profiles of TSG, (a) before and (b) after glassblowing. Glassblowing creates extremely smooth (0.2 ppm relative roughness) TSG structures.

glassblown samples showed a two-fold improvement in surface roughness, down to 0.23 nm Sa, Fig. 7(a). We also observed that the angstrom level scratches in Fig. 7(b), associated with the lapping operation, disappeared after glassblowing, Fig. 7(a), confirming the hypothesis.

Two-fold improvement in surface roughness is attributed to viscous flow of the glass layer and the associated surface tension forces. As the glassblowing is performed above the glass softening temperature, TSG device layer becomes viscous and the surface tension forces become active, working towards minimizing the surface area of the glass structure. This creates an effect analogous to "stretching out" the wrinkles on the surface, lowering the surface roughness.

4.2. Material composition

For resonant and optical applications, it is critical that TSG retains its original material composition and properties after glassblowing, which are structural integrity, material uniformity and optical transparency. We found that glassblowing temperature and the rate of cooling are the most important parameters that affect the quality of the TSG layer after glassblowing.

The structure in Fig. 8 was glassblown using a conventional high temperature furnace at 1600 °C, which does not allow removal of the samples at elevated temperatures. For this reason, the structure was left to cool-down to room temperature over an 8 h period. Recrystallization as well as micro-cracks were observed on the surface. In order to establish the nature of the recrystallization electron dispersive spectroscopy (EDS) was employed. Philips XL-30 FEG SEM with a Thermo Scientific UltraDry silicon drift X-ray detector was used for EDS characterization. An acceleration voltage of 10 kV was used at 10 mm working distance, and samples were coated with 5 nm of sputtered iridium to prevent charging.

EDS analysis of the crystals in Fig. 8 revealed higher concentrations of titanium, implying that TiO_2 is exsolving from the SiO_2/TiO_2

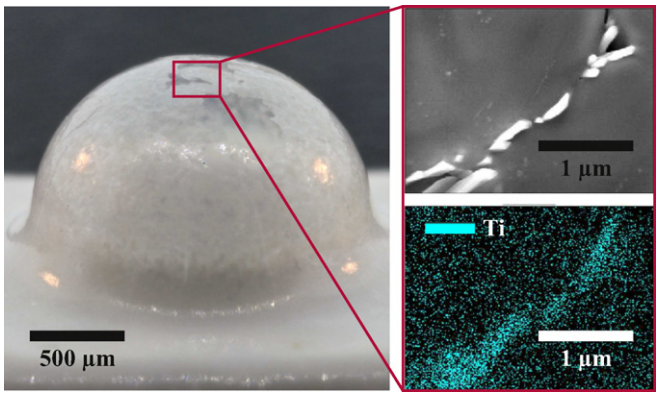

Fig. 8. Slow cooling of TSG (>8 h) causes recrystallization.

matrix. In contrast, the structure in Fig. 9 was glassblown using rapid cooling by bringing the temperature of the sample from 1600 to 1700 °C to ~200 °C within a minute. No micro-cracks or recrystallization were observed, as can be validated by the optical transparency. EDS spectral plots showed homogeneous SiO_2 and TiO_2 distribution in Fig. 9 as opposed to heterogeneous distribution in Fig. 8. The absence of recrystallization makes rapid cooling an essential step in micro-glassblowing of fused quartz and TSG.

EDS was used to obtain the spectral signatures of TSG before and after glassblowing. No change in the composition of TSG was observed after glassblowing, Fig. 10. EDS spectrums also revealed 7–8 weight percent of TiO_2 in TSG, which is in agreement with the nominal TiO_2 concentration of Corning ULE TSG.

4.3. Structural symmetry

For whole-angle gyroscope operation, a highly symmetric resonator structure is required as symmetry directly affects factors such as frequency split (Δf) and damping mismatch ($\Delta\tau^{-1}$) between degenerate $n=2$ wineglass modes. In order to evaluate the symmetry of the micro-glassblown structures image processing software in conjunction with scanning electron microscopy (SEM) was used.

Image processing techniques have previously been used for characterization of micro-scale features such as droplet interface shapes for microarray plates [17] and hemispherical resonators [18]. Following a similar approach, top-down view of the glassblown structure was first captured on a Hitachi 4700/EDAX SEM. To prevent charging of the dielectric glassblown structure due to the beam current, acceleration voltage was lowered to 1 kV and emission current to 10 μA. Images were captured at a magnification of 35× and saved at a resolution of 2560 × 1920 pixels. In

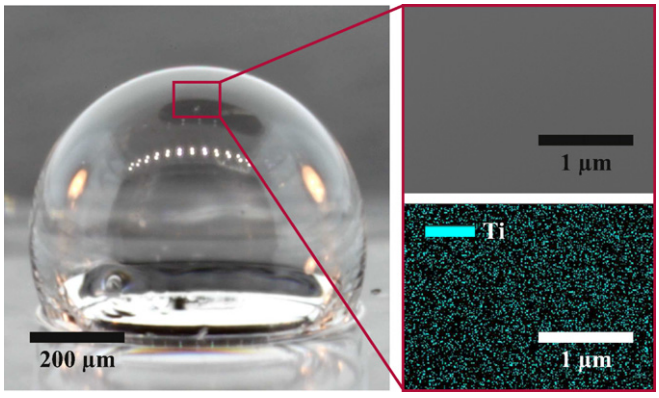

Fig. 9. Glassblowing with rapid cooling of TSG (<1 min) prevents recrystallization.

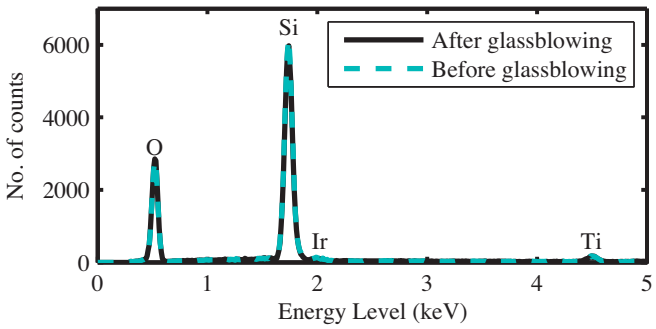

(a) EDS spectral analysis of ULE TSG.

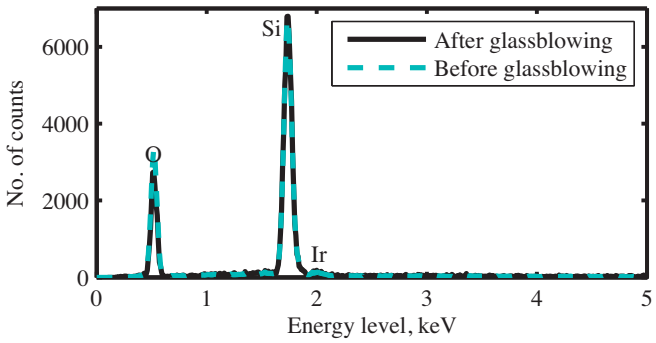

(b) EDS spectral analysis of fused quartz.

Fig. 10. EDS spectral analysis of TSG and fused quartz reveals that composition of the material does not change after glassblowing. (a) EDS spectral analysis of ULE TSG. (b) EDS spectral analysis of fused quartz.

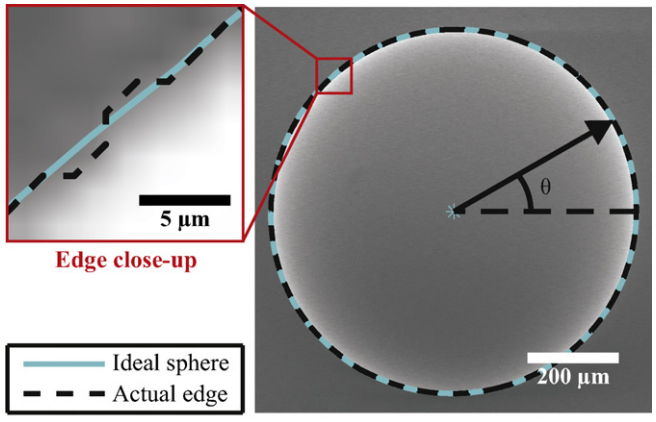

(a) Least squares fit to the perimeter of a fused quartz shell

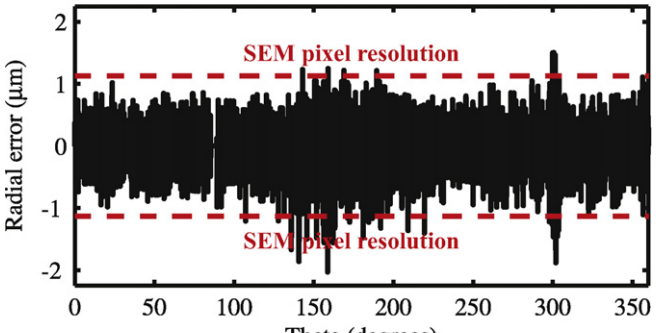

(b) Deviation from an ideal sphere along the perimeter

Fig. 11. Radial deviation from an ideal sphere, obtained through an edge-detection algorithm applied to the SEM image. (a) Least squares fit to the perimeter of a fused quartz shell and (b) deviation from an ideal sphere along the perimeter.

order to trace the edges of glassblown structure the image was converted to monochrome. The Otsu [19] method was used to find the grayscale threshold used in conversion from grayscale to monochrome. Shape distortions due to sample tilt or beam tilt, wobbling effect or non-uniform brightness and contrast was minimized by introducing a calibration step. This was achieved by mounting a photolithographically patterned calibration target next to the sample and cancelling out the common errors between the two.

An ideal circle was fitted to the actual edge using a least-squares (L-S) approach. Levenberg–Marquardt (LM) [20] algorithm was used for solving the L-S fit. A top-down SEM view of the spherical shell structure is shown in Fig. 11(a) with the superimposed traces of the actual edge and the ideal sphere. Radial error was calculated as the deviation of actual edge from the ideal sphere. The radial error with respect to the angle Theta is plotted in Fig. 11(b). The standard deviation of radial error was found to be 0.403 µm, which gives a relative error of ~500 ppm for the ~800 µm diameter sphere. The error falls below the SEM pixel resolution of 1.129 µm indicating that the structure is showing absolute symmetry within the capabilities of the SEM.

5. Conclusions

A new high temperature micro-glassblowing process for batch fabrication of 3-D low internal loss fused quartz and ULE TSG wineglass structures was developed and experimentally demonstrated. The process was enabled by the development of an in-house high temperature glassblowing capability of 1800 °C with a cooling rate of >500 °C/min and plasma activated fusion bonding of TSG to fused quartz. EDS spectral analysis of TSG before and after glassblowing revealed that the material retained its properties after glassblowing with no recrystallization or change in glass composition. AFM surface scans of the glassblown structures showed surface roughness of 0.23 nm Sa, which is 2× smaller than the roughness of the optically smooth device wafer. A novel inverted-wineglass architecture was also implemented, providing self-aligned stem structures. The method may enable new classes of TSG/fused quartz MEMS devices with atomically smooth surfaces, intrinsically low internal losses (Q_{TED} > 5E+10) and highly symmetric structures (radial error <500 ppm).

Wafer-scale nature of the micro-glassblowing process allows integration with existing MEMS technologies. Examples include deposition of conductive thin films before or after glassblowing [12] and bonding of wafers with separately fabricated optical waveguides or silicon-on-insulator (SOI) electrode structures onto the glassblown fused quartz/TSG wafers. Main areas of future work include experimental characterization of various stem designs, investigation of optical properties and integration of MEMS electrode structures for electrostatic transduction.

Acknowledgements

This material is based upon work supported by DARPA/SPAWAR under grant N66001-10-1-4074 & DARPA/AMRDEC grant W31P4Q-11-1-0006 (Program Manager Dr. Tayo Akinwande). Devices were designed and tested in UCI MicroSystems Lab. Authors would like to thank UCI INRF staff Jake Hes, Mo Kebaili, Vu Phan and Lifeng Zheng for their help and valuable suggestions on the fabrication aspects of the project.

References

[1] M. Weinberg, R. Candler, S. Chandorkar, J. Varsanik, T. Kenny, A. Duwel, Energy loss in MEMS resonators and the impact on inertial and RF devices, in: Solid-State Sensors, Actuators and Microsystems Conference, TRANSDUCERS 2009. International, Vol. 1, IEEE, 2009, pp. 688–695.

[2] D.M. Rozelle, The hemispherical resonator gyro: from wineglass to the planets, in: Proc. AAS/AIAA Space Flight Mechanics Meeting, 2009, pp. 1157–1178.
[3] L.D. Sorenson, X. Gao, F. Ayazi, 3-D micromachined hemispherical shell resonators with integrated capacitive transducers, in: IEEE MEMS 2012 Conference no., February, IEEE, 2012, pp. 168–171.
[4] L.C.L. Fegely, D.D.N. Hutchison, S.A. Bhave, Isotropic etching of 111 SCS for wafer-scale manufacturing of perfectly hemispherical silicon molds, in: 2011 16th International Solid-State Sensors, Actuators and Microsystems Conference, no. 1, IEEE, 2011, pp. 2295–2298.
[5] K. Visvanathan, T. Li, Y. Gianchandani, 3D-soule: a fabrication process for large scale integration and micromachining of spherical structures, in: IEEE 24th International Conference on Micro Electro Mechanical Systems (MEMS), IEEE, 2011, pp. 45–48.
[6] B. Sarac, G. Kumar, T. Hodges, S. Ding, Three-dimensional shell fabrication using blow molding of bulk metallic glass systems, Journal of Microelectromechanical Systems 20 (1) (2011) 28–36.
[7] I.P. Prikhodko, S.A. Zotov, A.A. Trusov, A.M. Shkel, Sub-degree-per-hour silicon MEMS rate sensor with 1 million Q-factor, in: 2011 16th International Solid-State Sensors, Actuators and Microsystems Conference, IEEE, 2011, pp. 2809–2812.
[8] T. Ray, H. Zhu, I. Elango, Characterzaton of KMPR 1025 as a masking layer for deep reactive ion etching of fused silica, in: IEEE MEMS 2012 Conference, Cancun, Mexico, 2011, pp. 213–216.
[9] K. Kolari, V. Saarela, S. Franssila, Deep plasma etching of glass for fluidic devices with different mask materials, Journal of Micromechanics and Microengineering 18 (6) (2008) 1–6.
[10] E.J. Eklund, A.M. Shkel, Glass blowing on a wafer level, Journal of Microelectromechanical Systems 16 (2) (2007) 232–239.
[11] S.A. Zotov, I.P. Prikhodko, A.A. Trusov, A.M. Shkel, 3-D micromachined spherical shell resonators with integrated electromagnetic and electrostatic transducers, in: Solid-State Sensors, Actuators, and Microsystems Workshop 2010, Hilton Head Island, South Carolina, USA, 2010, pp. 11–14.
[12] I.P. Prikhodko, S.A. Zotov, A.A. Trusov, A.M. Shkel, Microscale glass-blown three-dimensional spherical shell resonators, Journal of Microelectromechanical Systems 20 (3) (2011) 691–701.
[13] D. Senkal, I. Prikhodko, A. Trusov, Micromachined 3-D glass-blown wineglass structures for vibratory mems applications, in: Technologies for Future Micro-Nano Manufacturing Workshop 2011, Napa, CA, USA, 2011, pp. 166–169.
[14] D. Senkal, C. Raum, A. Trusov, Titania silicate/fused quartz glassblowing for 3-D fabrication of low internal loss wineglass micro-structures, in: Solid-State Sensors, Actuators, and Microsystems Workshop 2012, Hilton Head Island, South Carolina, USA, 2012, pp. 267–270.
[15] Comsol Multiphysics Package, http://www.comsol.com
[16] M. Eichler, B. Michel, P. Hennecke, M. Gabriel, C. Klages, Low-temperature direct bonding of borosilicate fused silica and functional coatings, Thin Films 33 (4) (2010) 339–348.
[17] M.J. Schertzer, M.J. Ahamed, R. Ben-Mrad, P. Lea, P.E. Sullivan, Characterizing the surface quality and droplet interface shape for microarray plates, Langmuir: The ACS journal of Surfaces and Colloids 28 (26) (2012) 9961–9966.
[18] P. Shao, L.D. Sorenson, X. Gao, F. Ayazi, Wineglass-on-a-chip, in: Solid-State Sensors, Actuators, and Microsystems Workshop 2012, Vol. 7, Hilton Head Island, South Carolina, USA, 2012, pp. 275–278.
[19] N. Otsu, A threshold selection method from grey-level histograms, IEEE Transactions on Systems Man and Cybernetics SMC-9 (1979) 62.
[20] M.I.A. Lourakis, A brief description of the Levenberg–Marquardt algorithm implemented by levmar, in: Foundation of Research and Technology 4, 2005, pp. 1–6.

Biographies

Doruk Senkal received B.S. degree in Mechanical Engineering from Middle East Technical University, Ankara, Turkey in 2007 and M.S. degree in Mechanical Engineering from Washington State University, Vancouver in 2009. He is currently a graduate student research assistant at University of California, Irvine Microsystems Laboratory, working toward a PhD in mechanical engineering. His research interests include design and control of magnetorheological brakes, 3-D MEMS resonators and micro-glassblowing of low expansion materials such as fused quartz and titania silicate glass.

Mohammed Jalal Ahamed received the M.A.Sc. and Ph.D. degrees in Mechanical Engineering from the University of Toronto, Toronto, Ontario, Canada in 2006 and 2011 respectively. He is currently a Post-doctoral fellow at University of California, Irvine, where he is developing 3-D microhemispherical resonators. His research interests include MEMS resonators, sensors, actuators, microfluidics and biomedical lab-on-a-chip technology.

Alexander A. Trusov received B.S. and M.S. degrees in applied mathematics and mechanics from the Moscow State University, Russia in 2004 and the M.S. and Ph.D. degrees in mechanical and aerospace engineering from the University of California, Irvine in 2006 and 2009, respectively. He is currently a project scientist in the Mechanical and Aerospace Department at the University of California, Irvine, where he serves as the PI and Co-PI on half a dozen DoD sponsored research programs. He is also responsible for teaching MAE 247/EECS 278 "MicroSystems Design" class at UCI. Dr. Trusov's research interests include design, modeling, fabrication, and vacuum packaging of micromachined inertial systems, design of characterization experiments, and statistical data processing and analysis. Dr. Trusov has published 15 journal and over 35 conference papers on MEMS and signal processing and has 1 U.S. patent (with 6 more pending) on MEMS design, fabrication, and control. His work on low dissipation MEMS gyroscopes received an Outstanding Paper award at Transducers 2011, Design Contest award at System-on-Chip Conference 2011, and the Best Paper award at IMAPS Device Packaging Conference 2012. He serves as a reviewer for major journals in the fields of MEMS and sensors and is a member of MEMS & Associated Microsystems organizing committee for the IMAPS Device Packaging 2011 and 2012 conferences. He is a member of the American Society of Mechanical Engineers (ASME) and the Institute of Electrical and Electronics Engineers (IEEE).

Andrei M. Shkel received the diploma degree (with excellence) in mechanics and mathematics from the Moscow State University, Moscow, Russia, in 1991, and the Ph.D. degree in Mechanical Engineering from the University of Wisconsin, Madison, in 1997. He is a program manager in the Microsystems Technology Office of the Defense Advanced Research Projects Agency (DARPA), Arlington, VA, where he is managing DARPA's investment portfolio in Microtechnology for Positioning, Navigation, and Timing (microPNT). He is serving in this capacity while on leave from his faculty position as a professor in the Department of Mechanical and Aerospace Engineering at the University of California, Irvine, where he is also the Director of the UCI Microsystems Laboratory. He is the holder of 18 U.S. and international patents. His professional interests are reflected in more than 160 publications. He is a recipient of the 2009 Research Award from the IEEE Sensors Council, the 2006 UCI Research Award, the 2005 NSF CAREER Award, and the 2002 George E. Brown, Jr., Award. He is an editor of the IEEE/ASME Journal of Microelectromechanical Systems (JMEMS).

Please cite this article in press as: D. Senkal, et al., High temperature micro-glassblowing process demonstrated on fused quartz and ULE TSG, Sens. Actuators A: Phys. (2013), http://dx.doi.org/10.1016/j.sna.2012.11.040